mass by plotting the product $M\theta^2$ so that they correspond to an average interatomic force constant in a central-force model of lattice vibrations. It is apparent that the force constant for hafnium is considerably larger than the force constants for the other three metals. The atomic volume of hafnium also is unusually small as shown in the second curve in the figure as a result of the lanthanide contraction which accompanies the filling of the $4f$ shell. This contraction is due to a stronger field acting upon the valence electrons as a result of the incomplete screening by the $4f$ electrons of the increased nuclear charge and results in increased binding forces. Thus the high force constant for hafnium is believed to be principally due to the lanthanide contraction. Electrons in both s and d bands contribute to the electronic specific heat. Since the s-wave functions are more penetrating, the bottom of the s band should be lowered with respect to the bottom of the d band by increasing nuclear charge. In terms of the two-band model then, this would result in a smaller number of electrons in the d band, and hence, a decreasing electronic specific heat with increasing nuclear charge. Strictly speaking, this is only true if a decrease in the density of states in the d band occurs with a decrease in the number of electrons in the band but experimental evidence from zirconium alloys indicates this to be a reasonable assumption. As a result of the lanthanide contraction, the s and d wave functions should overlap to a great extent in hafnium and, therefore, the density of states should be reduced still further. The figure shows that this effect must be small, however, compared to the shift in position of the s and d bands.

PHYSICAL REVIEW VOLUME 130, NUMBER 5 1 JUNE 1963

Electrically Induced Nuclear Resonance in Al_2O_3 (Ruby)

TOSHIMOTO KUSHIDA AND A. H. SILVER
Scientific Laboratory, Ford Motor Company, Dearborn, Michigan
(Received 28 January 1963)

The application of an electric field to a crystalline lattice will, in general, produce an optical mode distortion. This lattice distortion will contribute to the electric field gradient tensor at the positions of the various atoms in the lattice. By applying an oscillating electric field to a single crystal of α-Al_2O_3 we have induced $\Delta m = \pm 2$ transitions for the Al^{27} nuclear spins. These "quadrupole" transitions were observed with a nuclear double resonance technique at 4.2°K. An rf electric field orthogonal to the trigonal axis of the crystal induced an oscillating asymmetry parameter η in the electric field gradient tensor. The magnitude of η as determined from the transition probability is $1.5\times10^{-7}/(\mathrm{V/cm})$. The transient behavior as well as the steady-state populations were observed following the application and removal of the rf electric field. The initial slope of the signal following the application of the electric field was used to determine the quadrupole transition probability, and the remaining transient response was interpreted qualitatively in terms of the normal modes of the relaxation. These modes were derived from the rate equations which included the external driving terms. The line shape for the $\Delta m = \pm 2$ nuclear electric resonance was observed indirectly and is more than twice as broad as the dipolar lines with a distinct asymmetry. The width and shape are interpreted in terms of the nuclear dipole-dipole interaction.

I. INTRODUCTION

THE application of an electric field to a crystalline lattice will produce an optical mode distortion of the lattice. This electric polarization of the lattice will produce an associated internal electric field and its corresponding spacial derivatives. Bloembergen[1] has pointed out that for nuclei or paramagnetic ions in a lattice whose sites lack inversion symmetry, an externally applied electric field E produces a change in the quadrupole coupling constants or in the crystalline field splittings which are proportional to E. Such changes in the nuclear quadrupole coupling were first observed as a frequency shift or a broadening of the nuclear quadrupole resonance line.[2,3] This linear electric field shift has also been observed in paramagnetic resonance spectra.[4,5]

Bloembergen[1] also suggested that if an oscillating electric field whose frequency matches the resonance condition is applied, transitions may be induced at a rate proportional to E^2. This effect has been observed by means of a change in the nuclear free induction decay signal for Ga^{69}, Ga^{71}, and As^{75} in GaAs when electric quadrupole transitions, $\Delta m = \pm 2$, were induced by means of an external electric field.[6]

[1] N. Bloembergen, Science **133**, 1363 (1961).
[2] T. Kushida and K. Saiki, Phys. Rev. Letters **7**, 9 (1961).
[3] J. Armstrong, N. Bloembergen, and D. Gill, Phys. Rev. Letters **7**, 11 (1961).
[4] G. W. Ludwig and H. H. Woodbury, Phys. Rev. Letters **7**, 240 (1961); J. O. Artman and J. C. Murphy, Bull. Am. Phys. Soc. **7**, 14 (1962).
[5] E. B. Royce and N. Bloembergen, Bull. Am. Phys. Soc. **7**, 200 (1962). After completion of this experiment, Bloembergen has kindly informed us that R. Dixon has observed the dc electric field effect on Al^{27} NMR lines in Al_2O_3. This was accomplished by using as much as 300 kV/cm. We would like to acknowledge the valuable comment given by Professor N. Bloembergen.
[6] E. Brun, R. Hann, W. Pierce, and W. H. Tanttila, Phys. Rev. Letters **8**, 365 (1962).

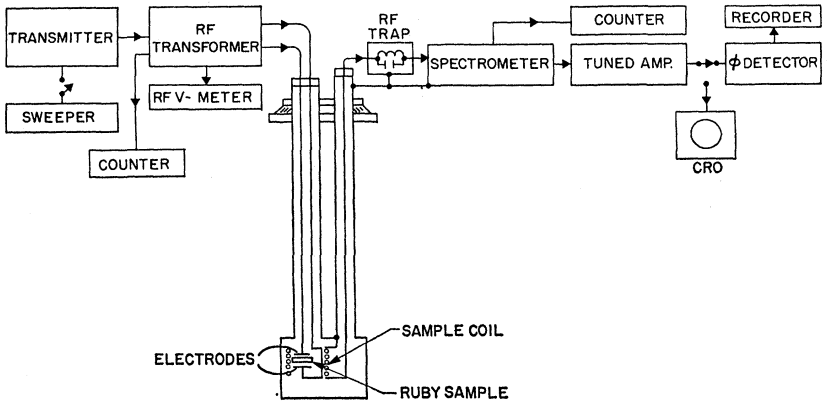

FIG. 1. Schematic drawing of the nuclear double resonance system to observe an electrically induced nuclear transition.

In the present experiment, we have observed electrically induced quadrupole transitions for Al^{27} in Al_2O_3 using a double resonance technique. With the chosen geometry, the electric field produces an asymmetry η in the field gradient tensor. The measured transition probability gives the magnitude of the induced η.

The nuclear orientation energy can be expressed by the following Hamiltonian, if an external magnetic field H_0 is parallel to the direction of the largest principal axis of the field gradient tensor,

$$\mathcal{H}=-H_0\gamma I_z+\frac{e^2Qq}{4I(2I-1)}[3I_z^2-I^2+\tfrac{1}{2}\eta(I_+^2+I_-^2)], \quad (1)$$

where conventional notations are used and the direction of H_0 is chosen as the z axis.

Since the first (Zeeman) term is larger than the second (quadrupole) term in the present case, six equally spaced Zeeman levels corresponding to $I=5/2$ for Al^{27} are perturbed by the quadrupole term giving five nuclear magnetic dipole resonance (NMR) lines which correspond to $\Delta m=\pm 1$ transitions.[7] Since an Al_2O_3 (α-Al_2O_3) crystal has threefold symmetry about its c axis which is parallel to the direction of the principal axis of the field gradient tensor z, η is zero when the external electric field is absent. If the oscillating electric field is applied in the xy plane, the local distortion of the environment about the Al ion will produce an oscillating asymmetry parameter. This can produce the quadrupole transitions $\Delta m=\pm 2$, since $(I_+^2+I_-^2)$ has nonvanishing matrix elements only for $\Delta m=\pm 2$ in the representation which diagonalizes the remaining time-independent terms.

Since this electrically induced transition disturbs the nuclear populations among these energy levels, this transition can be observed as an intensity change or as a reversal of the intensity in the NMR signal which corresponds to one of the $\Delta m=\pm 1$ transitions.

II. EXPERIMENTAL METHOD AND RESULTS

The nuclear magnetic resonance line of Al^{27} was observed using a conventional modified Pound-Knight-Watkins spectrometer as is shown in Fig. 1. In order to prevent the interference from the strong oscillating electric field, whose frequency is roughly twice that of the spectrometer frequency, an rf trap[8] was inserted between the sample coil and the spectrometer. The experiment was carried out at liquid-He temperature. The steady-state signal and the relatively slow part of transient nuclear signals were displayed on the recorder, and the faster part was observed on the CRO screen of a Tektronix 545A.

The sample was 0.01% Cr-doped single-crystal disk of ruby, Al_2O_3 with 11.2 mm diam and 1.9 mm thickness. The c axis was in the disk plane, and gold films were sputtered on these planes as electrodes. The axis of the spectrometer rf coil was perpendicular to the electrodes. The alignment of the c axis of the crystal to the direction of the magnetic field H_0 was accomplished by observing the quadrupole splittings of the NMR lines with an accuracy of one degree. The misalignment of the crystal may cause a slight mixing of the energy states, which may permit weak magnetic dipole transitions between $\Delta m=\pm 2$ levels. Since the oscillating electric field is accompanied by a displacement current, the oscillating magnetic field produced by this current may induce weak $\Delta m=\pm 2$ magnetic transitions. This effect of the displacement current was actually observed in this laboratory for a similar but preliminary electric field experiment using a $NaBrO_3$ single crystal. The $(\pm 3/2 \rightleftarrows \pm 1/2)$ or the $(\pm 3/2 \rightleftarrows \mp 1/2)$ transition between Zeeman-split levels of Br^{81} was excited by the oscillating electric field, while the $(+1/2 \rightleftarrows -1/2)$ transition was monitored with the spectrometer at liquid-nitrogen temperature. A strong enhancement in the spectrometer signal was observed only when the $(\pm 3/2 \rightleftarrows \pm 1/2)$ transition was excited. No effect was observed for the $(\pm 3/2 \rightleftarrows \mp 1/2)$ transition. Since the transition probabilities for these two transitions are expected to be about the same for the electric excitation, the observed effect is associated with the magnetic transition induced by the magnetic field associated with the displacement current.

[7] R. V. Pound, Phys. Rev. **79**, 123 (1950).

[8] A. H. Silver, J. Phys. Chem. Solids **23**, 273 (1962).

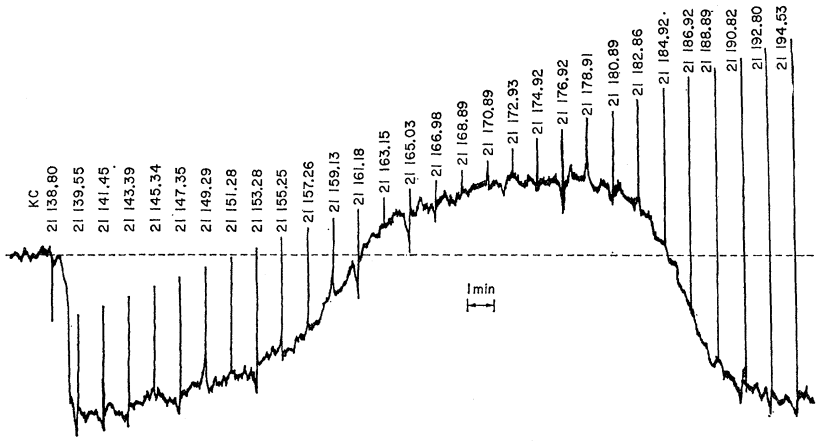

FIG. 2. The nuclear electric resonance line ($5/2 \rightleftarrows 1/2$) observed as an intensity change in the monitor NMR signal ($5/2 \rightleftarrows 3/2$). The frequency markers indicate the frequency of the rf electric field. The signal to the left of the frequency marker 21 138.80 kc/sec shows the zero point of the system, the deflection between the markers 21 138.80 and 21 139.55 corresponds to the amplitude of the monitor NMR signal when the rf electric field does not hit the resonance frequency. As the frequency of the electric field increases, the monitor signal decreases, and near the center of the electric resonance the monitor signal goes beyond the zero point indicating the presence of an induced emission. The voltage of the rf electric field across the sample (1.9 mm thick) is 280 V *p-p*.

In order to observe the electric field transition using the present technique, the spin-lattice relaxation time T_1 must be longer than the inverse of the transition probability. The effect for the Al_2O_3 crystal was not observed at liquid-nitrogen temperature, because T_1 is not long enough at this temperature. Our attempt to observe this effect at liquid-He temperature for the $NaBrO_3$ single crystal was unsuccessful with the present setup, because the ($\pm 1/2 \rightleftarrows \mp 1/2$) line was very strongly saturated at this temperature even with the weakest possible rf level of the spectrometer. The effect would be observed if a bridge spectrometer or a Robinson-type spectrometer[9] were used to reduce the rf level further.

We will rule out the effects of the displacement currents in our present experiments in Al_2O_3 for the following reasons: (i) The magnitude of the displacement current for the Al_2O_3 experiment was about one order of magnitude smaller than the case of the $NaBrO_3$ experiment, because the electric field frequencies used in these experiments were about 20 and 150 Mc/sec, respectively. Therefore, the transition probability accompanied by this effect is different by two orders of magnitude. (ii) If this effect is responsible for the observed $\Delta m = \pm 2$ transitions in the present experiment, the transition probability must depend on the mixing rate of the states which make this magnetic transition possible. Therefore, the intensity of the observed transitions ought to depend strongly on the alignment of the crystal. The observed intensity, however, did not change with slight changes in the crystal axis orientation.

A 180-W Heathkit Apache transmitter was used to provide the electric field in conjunction with an rf transformer. Since the tuning range of this transmitter is relatively small (21.000–21.450 Mc/sec), the magnetic field was so adjusted as to satisfy one of the $\Delta m = \pm 2$ transitions for this frequency. The magnetic field was modulated with 280 cps.

A "nuclear electric resonance" line thus observed is shown in Fig. 2. Here the spectrometer frequency was adjusted to the ($5/2 \rightleftarrows 3/2$) line so that the recorder signal gives the negative maximum deflection in the derivative curve. The frequency of the Apache transmitter was swept over the ($5/2 \rightleftarrows 1/2$) transition frequency. The frequency markers in the figure indicate the transmitter frequencies. The off-resonance position, namely, the recorder indication when neither the spectrometer nor the transmitter frequency satisfies the resonance conditions, is indicated at the left part of the curve. The spectrometer signal decreases when approaching the resonance frequency for the $\Delta m = \pm 2$ transition, and it reverses at the center of the line. This shows that the population at the 3/2 level was made larger than the lower-lying 5/2 level by the electric field pumping.

It is noted that the apparent linewidth is considerably larger than that of the usual NMR lines, which are about 8 kc/sec,[10] and the line shape is not symmetric.

Now the transient response of the NMR monitor signal was investigated. Figure 3 shows a typical transient response curve schematically. First, the static magnetic field was kept at an off-resonance value for more than 10 min in order to permit the nuclear spin system to reach its equilibrium state. The recorder trace gives the zero point of the system, which corresponds to the left part of A in the figure.

The magnetic field was flipped to the value which gives the maximum deflection of the derivative curve of the NMR line (A at Fig. 3). After the intensity of the nuclear signal reaches equilibrium at a partially saturated value, the pumping electric field, whose frequency was previously adjusted to the center of the $\Delta m = \pm 2$ transition, was switched on (B). This partial saturation is not necessary for the observation of the electric field effect and the interpretation of the observed curve becomes simpler if the rf level of the spectrometer is kept sufficiently small so as to avoid saturation. It was necessary, however, to keep the rf level at the partially saturating value for the present setup, in order to obtain a good signal-to-noise ratio with a relatively short time constant of 2.5 sec for the lock-in amplifier.

[9] F. N. H. Robinson, J. Sci. Instr. **36**, 481 (1959).

[10] A. H. Silver, T. Kushida, and J. Lambe, Phys. Rev. **125**, 1147 (1962).

When the pumping field is switched on the nuclear signal amplitude changes rapidly at first and then gradually reaches a new stationary value. Incidentally, the electric resonance shown in Fig. 2 was obtained with a sufficiently slow sweep speed for the transmitter frequency so that the observed resonance curve follows this stationary value as a function of the transmitter frequency.

The shape of the transient curve depends on which NMR line one is observing, which transition is saturated by the electric pumping, and the value of both pumping voltage and the spectrometer rf level.

A general consideration which will be shown later indicates that the response curve can be described as a linear combination of at most five normal relaxation modes for the case of spin 5/2. Each mode has a characteristic time dependence $\exp(-\lambda^{(k)}t)$, where the $\lambda^{(k)}$ ($k=1, 2, \cdots, 5$) are the inverse of the five characteristic relaxation times, respectively. It is noted that any number of external driving fields and/or spin-lattice relaxation mechanisms does not increase the number of the relaxation modes. They only change the magnitude of $\lambda^{(k)}$, and the initial condition changes the amplitude of the normal modes of relaxation.

Since the over-all response time of the apparatus including the spectrometer through the recorder was about 2.5 sec, the initial fast response of the nuclear signal was masked by the equipment response time. Therefore, this initial part was displayed separately on the CRO screen as shown in Fig. 1, without using the phase detector and the recorder. The over all response time of this latter system was less than 1 sec and was predominantly determined by the bandwidth of the tuned amplifier.

After the spin system attained equilibrium with the pumping field, the electric field was turned off (C in Fig. 3), and the recovery curve to the equilibrium spin distribution with the rf magnetic field was recorded, ($C-D$). At D the magnetic field was changed to the off-resonance position to check the zero point of the system.

The transient curves were observed for all five NMR lines when the $(5/2 \rightleftarrows 1/2)$ or the $(3/2 \rightleftarrows -1/2)$ pumping electric field was applied, since the $(m \rightleftarrows m-2)$ pumping gives the same results for the $(m' \rightleftarrows m'-1)$ monitor signal as the $[-m \rightleftarrows -(m-2)]$ electric transition produces to the $[-m' \rightleftarrows -(m'-1)]$ magnetic transition.

An appreciable electric transition probability was observed for an rf voltage of about 50 V(p-p) across the sample, the maximum applied voltage being 280 V across the sample whose thickness was 1.9 mm. The transient curves for the $(5/2 \rightleftarrows 1/2)$ and the $(3/2 \rightleftarrows -1/2)$ pumping are shown in Figs. 4 and 5, respectively.

The fast part of the response curve right after the turn-on of the pumping was investigated as a function of the pumping voltage by taking pictures of the CRO signals.

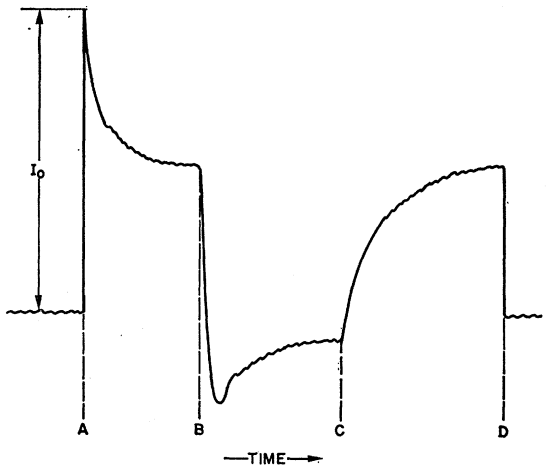

FIG. 3. Schematic plot of the transient response of the monitor NMR signal. The left side of A: off-resonance; A: the magnetic field is brought to the resonance value of the monitor NMR so that the maximum deflection I_0 in the derivative curve of the line is observed; B: the rf electric field is turned on; C: the electric field off; D: the magnetic field is flipped off.

The initial slope of the response curve,

$$-I_0^{-1}(dI/dt)_{t=0+},$$

is shown as a function of the square of the pumping field, E^2, in Fig. 6. Here the amplitude of the signal is normalized with respect to the nuclear signal without the electric field or saturation effect, I_0 (see Fig. 3). In Fig. 6, $\oplus$ indicates the case where $\nu_E=(3/2 \rightleftarrows -1/2)$ and $\nu_M=(3/2 \rightleftarrows 1/2)$, and $\triangle$ corresponds to $\nu_E=(3/2 \rightleftarrows -1/2)$ and $\nu_M=(1/2 \rightleftarrows -1/2)$. The straight line represents $-I_0^{-1}(dI/dt)_{t=0+}=1.0\times10^{-6}E^2$, where E is the applied field expressed in V/cm.

III. RATE EQUATIONS AND THEIR SOLUTIONS

In order to interpret the experimental results described in the previous section and derive the magnitude of the distortion in the field gradient tensor caused by the electric field, it is necessary to analyze the relaxation rate equations which include the spin-lattice relaxation parameters, the rf magnetic excitation, and the rf electric field excitation.

The population difference N_j between adjacent levels $j+1/2$ and $j-1/2$ is described by a series of rate equations. If the energy level separations are nearly equal so that the equilibrium population differences N_j^0 can be approximated by a mean value N^0 but they are different to such an extent that completely separate NMR lines are observed, a normalized population difference $n_j=N_j/N^0$ can be described by[8]

$$dn_j/dt=\sum_i(A_{ji}+B_{ji})n_i-\sum_i A_{ji}, \qquad (2)$$

where the A_{ji}'s are the spin-lattice relaxation matrix,

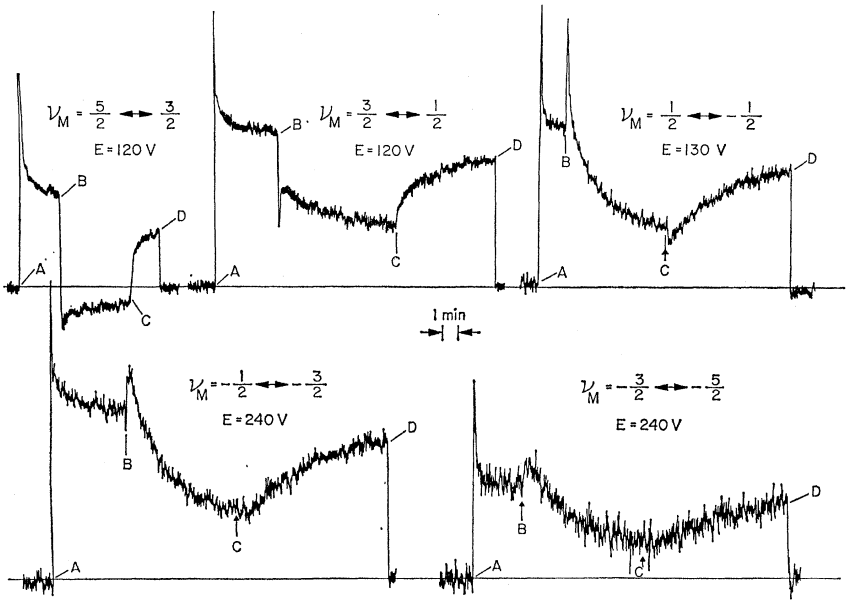

FIG. 4. The transient response curves of the monitor NMR signals when the electric rf field is applied to the $(5/2 \rightleftarrows 1/2)$ spacing. ν_M in the figure indicates the NMR transition which is monitored. E is the rf p-p voltage across the sample (1.9 mm thick). A, B, C, and D have the same meanings as in Fig. 3.

and B_{ji}'s are the matrix elements which describe the external driving fields.

The solutions of these equations have been treated for a few cases: (i) The case where $B_{ji}=0$ and the A_{ji}'s are a quadrupole relaxation, has been considered by Andrew and Tunstall[11]; (ii) one of the authors[8] solved these equations numerically when the A_{ji}'s are the quadrupole relaxation and the B_{ji}'s are caused by an acoustic excitation; and (iii) Simmons *et al.*[12] have developed a general theory for the case when the A_{ji}'s are caused by paramagnetic impurities and there is no B_{ji} term.

The elements of the relaxation matrix, A_{ji}, are c numbers when the relaxation is caused by quadrupole and/or direct paramagnetic relaxation.[8,11,12] If spin diffusion is responsible for the relaxation, Simmons *et al.*[12] have shown that the elements of A_{ji} are proportional to the operator ∇^2. However, this operator can be approximated by c number matrix elements as will be shown in the Appendix. We shall treat the elements A_{ji} as c numbers throughout the remainder of this paper.

A. Steady-State Solution

If the only driving field is to excite $\Delta m=\pm 1$ transition, an important example being the rf magnetic field, the matrix B has the form,[8]

$$\begin{aligned} B_{ll} &= -2K, \\ B_{l,l+1} &= B_{l,l-1} = K, \end{aligned} \tag{3}$$

and all other B_{ji} are zero. Here the driving field is applied to the lth energy spacing, and K is its transition probability.

If we observe the lth population difference using a spectrometer, the signal intensity will be,

$$n_l = [1+K(H_{ll}/\Delta)]^{-1}, \tag{4}$$

where $\Delta = \det A_{ji}$, and H_{ll} is

$$H_{ll} = \det \begin{bmatrix} & & l & \\ & & \vdots & \\ \cdots A_{l+2,l+1} & & 0 & A_{l+2,l-1}\cdots \\ A_{l+1,l+1} & & 1 & A_{l+1,l-1} \\ A_{l,l+1} & & -2 & A_{l,l-1}\cdots \\ A_{l-1,l+1} & & 1 & A_{l-1,l-1} \\ A_{l-2,l+1} & & 0 & A_{l-2,l-1} \\ \cdots & & \cdots & \cdots \end{bmatrix} l. \tag{5}$$

Equation (4) is the formal extension of the familiar saturation equation for $I=1/2$,[13]

$$n = [1+\tfrac{1}{2}\gamma^2 H_1^2 T_1 g(\nu)]^{-1}. \tag{6}$$

Generally, the population difference at the kth spacing is

$$n_k = 1 - KH_{kl}/(\Delta + H_{ll}K), \tag{7}$$

where H_{kl} is the determinant of the matrix A_{ji} whose kth column is replaced by the following column,

$$\begin{matrix} 0 \\ \vdots \\ 0 \\ 1\cdots l+1 \\ -2\cdots l \\ 1\cdots l-1. \\ 0 \\ \vdots \\ 0 \end{matrix} \tag{8}$$

[11] E. R. Andrew and D. P. Tunstall, Proc. Phys. Soc. (London) **78**, 1 (1961).

[12] W. W. Simmons, W. J. O'Sullivan, and W. A. Robinson, Phys. Rev. **127**, 1168 (1962).

[13] N. Bloembergen, E. M. Purcell, and R. V. Pound, Phys. Rev. **73**, 679 (1948).

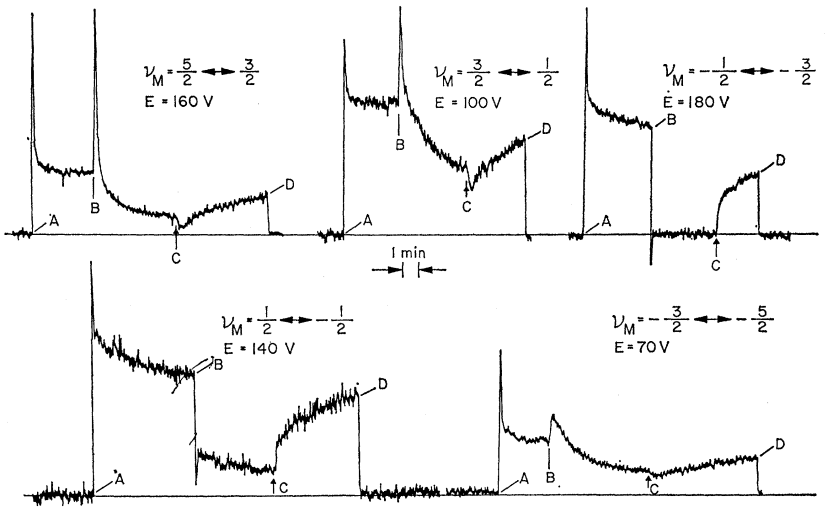

FIG. 5. The transient response curves of the monitor NMR signals when the electric rf field is applied to the $(3/2 \rightleftarrows -1/2)$ level. The notation is the same as in Fig. 4.

Equation (7) includes Eq. (4) as the special case of $k=l$. It must be noted that in Eq. (7)

$$H_{kl}=0 \quad \text{for} \quad k\neq l, \tag{9}$$

if the thermal relaxation mechanism produces only $\Delta m=\pm 1$ transitions, because in this case the lth column of the relaxation matrix A_{ji} has the form

$$\begin{matrix} 0 \\ \vdots \\ 0 \\ -w\cdots l+1 \\ 2w\cdots l \\ -w\cdots l-1, \\ 0 \\ \vdots \\ 0 \end{matrix} \tag{10}$$

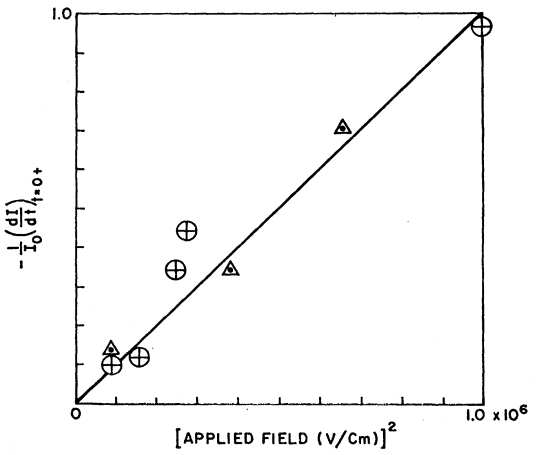

FIG. 6. Initial slope of the amplitude of the monitor NMR signal as a function of the square of the applied rf electric field. ⊕: $\nu_E=(3/2 \rightleftarrows -1/2)$ and $\nu_M=(3/2 \rightleftarrows 1/2)$. △: $\nu_E=3/2 \rightleftarrows -1/2)$ and $\nu_M=(1/2 \rightleftarrows -1/2)$.

where w is the appropriate thermal transition probability.

If the driving field corresponds to the transition $\Delta m=\pm 2$, examples being the present electric field or acoustic $\Delta m=\pm 2$ excitation, the matrix B is[8]

$$B=\begin{matrix} & l+1 & l & & \\ & \vdots & \vdots & & \\ \cdots 0 & 0 & 0 & 0 & \\ 0 & P & P & 0\cdots & l+2 \\ 0 & -P & -P & 0\cdots & l+1 \\ 0 & -P & -P & 0\cdots & l \\ 0 & P & P & 0\cdots & l-1, \\ 0 & 0 & 0 & 0\cdots & \\ \cdots & \cdots & \cdots & \cdots & \end{matrix} \tag{11}$$

where the driving field is applied to the energy spacing $l\rightarrow(l+1)$, and P is its transition probability.

If the jth population difference n_j is observed with a sufficiently weak rf magnetic field,

$$n_j=1-\frac{2P_{jl}P}{\Delta+(P_{l+1l}+P_{ll})P}, \tag{12}$$

where P_{jl} is the determinant of the matrix A_{ji} whose jth column is replaced by the following column,

$$\begin{matrix} 0 \\ \vdots \\ 0 \\ 1\cdots l+2 \\ -1\cdots l+1 \\ -1\cdots l \\ 1\cdots l-1. \\ 0 \\ \vdots \\ 0 \end{matrix} \tag{13}$$

If the observing rf power level is not small, which is the

present case, B_{ji} is the sum of Eqs. (3) and (11), the calculation is straightforward and the result is

$$n_j=\frac{\Delta+(P_{ll}+P_{l+1l}-2P_{jl})P}{\Delta+(P_{ll}+P_{l+1l})P+[(HP)_{jl,jl}+(HP)_{jl+1,jl}]KP+H_{jj}K}. \tag{14}$$

Here $(HP)_{jl,jl}$ and $(HP)_{jl+1,jl}$ are the determinants of A_{ji} whose j and lth and j and $(l+1)$th columns, respectively, are replaced as follows:

$$(HP)_{jl,jl}=\det\begin{bmatrix} & j & l & \\ \cdots & 0\cdots & 0\cdots & \\ & \vdots & \vdots & \\ & 0 & 0 & \\ & 1 & 0 & \\ & -2\cdots & 0\cdots & j \\ & 1 & 0 & \\ & 0 & 0 & \\ & \vdots & \vdots & \\ & & 1 & \\ & & -1 & \\ & & -1 & l \\ & & 1 & \\ & & 0 & \\ & & \vdots & \\ \cdots & 0\cdots & 0\cdots & \end{bmatrix} \quad \text{for} \quad j\neq l, \tag{15}$$

$$(HP)_{jl,jl}=0 \quad \text{for} \quad j=l.$$

$$(HP)_{jl+1,jl}=\det\begin{bmatrix} & j & l+1 & \\ \cdots & 0\cdots & 0 & \\ & \vdots & \vdots & \\ & 0 & 0 & \\ & 1 & 0 & \\ & -2\cdots & 0\cdots & j \\ & 1 & 0 & \\ & 0 & 0 & \\ & \vdots & \vdots & \\ & & 0 & \\ & & 1 & \\ & & -1 & \\ & & -1 & l \\ & & 1 & \\ & & 0 & \\ & & \vdots & \\ & & 0 & \end{bmatrix} \quad \text{for} \quad j\neq l+1, \tag{16}$$

$$(HP)_{jl+1,jl}=0 \quad \text{for} \quad j=l+1.$$

The successive saturation experiments, therefore, give a combination of some of the co-factors in the relaxation matrix. When the A_{ij}'s contain only a few unknown parameters, such steady-state saturation experiments might be sufficient to determine these parameters. In general, however, these experiments do not give full information to derive each component of A_{ij}.

B. Transient Solution

The general transient behavior of the solutions of the rate equations (2) have been discussed when there is no external driving term B_{ij} by Andrew and Tunstall[11] and by Simmons *et al.*[12] Their results can easily be extended so as to include the effect of B_{ij} by taking the time derivative of Eq. (2),

$$d^2n_j/dt^2=\sum_i(A_{ji}+B_{ji})dn_i/dt. \tag{17}$$

The solutions of Eq. (17) are

$$dn_j/dt=\sum_k a_j^{(k)}\exp(-\lambda^{(k)}t), \tag{18}$$

and the solutions of Eq. (2) are, therefore,

$$n_j(t)=\sum_k-\frac{a_j^{(k)}}{\lambda^{(k)}}\exp(-\lambda^{(k)}t)+n_j(\infty). \tag{19}$$

Here the $n_j(\infty)$'s are the steady-state solutions obtained in the previous section; $\lambda^{(k)}$ and $a_j^{(k)}$ are the eigenvalues and the eigenfunctions of the matrix $(A_{ji}+B_{ji})$, namely,

$$\sum_i(A_{ji}+B_{ji}+\delta_{ji}\lambda^{(k)})a_i^{(k)}=0. \tag{20}$$

Therefore, the transient solutions of Eq. (2) are a superposition of the normal mode relaxations which are characterized by $\lambda^{(k)}$ in Eq. (20). Since the number of k is at most equal to $2I$, any transient change of the observed signal must be expressed by a linear combination of at most $2I$ relaxation functions, $\exp(-\lambda^{(k)}t)$.

The ratios among $a_j^{(k)}$'s with the same k but different j values are determined as the eigenfunctions in Eq. (20), and the magnitudes of the $a_j^{(k)}$ are determined by the initial conditions. Since only the ratios among $a_j^{(k)}$'s with the same k are determined by Eq. (20), Eq. (19) can be rewritten as

$$n_j(t)=a_j^{(k)}\exp(-\lambda^{(k)}t)+n_j(\infty), \tag{21}$$

by rewriting $-a_j^{(k)}/\lambda^{(k)}$ in Eq. (19) as $a_j^{(k)}$.

If the transient curves are obtained experimentally for every n_j, fitting these curves to Eq. (19) will, in principle, determine all the relaxation constants $\lambda^{(k)}$ and all $(2I\times 2I)$ values of $a_j^{(k)}$. These values permit a determination of all the matrix elements of $A_{ji}+B_{ji}$ through Eq. (20).

These results are a generalization of those shown in references 11 and 12 so as to include the external driving fields.

C. Initial Rise Time

Another important quantity derived from the rate equations (2) is the initial rise time (or initial slope) of n_j when one of the external driving fields is suddenly turned on. From Eq. (2) we can write

$$dn_j/dt=\sum_i(A_{ji}+B_{ji}^{(1)}+B_{ji}^{(2)})n_i(t)-\sum_i A_{ji},$$

where $B_{ji}^{(1)}$ is the external driving field which is continuously present, and $B_{ji}^{(2)}$ is the one which is turned on at $t=0$.

If the system has been in a stationary state before $t=0$,

$$(dn_j/dt)_{t<0}=\sum_i(A_{ji}+B_{ji}^{(1)})n_i-\sum_i A_{ji}=0,$$

therefore,

$$(dn_j/dt)_{t=0+}=\sum_i B_{ji}^{(2)}n_i(0). \tag{22}$$

Here $(dn_j/dt)_{t=0+}$ is the initial rise rate (slope) right after $B_{ji}^{(2)}$ is switched on. The transition probability caused by the driving field $B_{ji}^{(2)}$ can be directly obtained from Eq. (22) using such relations as Eq. (3) for $\Delta m=\pm1$ excitation and Eq. (11) for $\Delta m=\pm2$ excitation if the initial values $n_j(0)$ are known.

IV. ANALYSIS OF EXPERIMENTAL RESULTS

A. Initial Slope

The nuclear transition probability caused by the external electric field, which is the main interest of this paper, is most directly obtained from the initial slope observation.

Equation (22) with the matrix element $B_{ji}^{(2)}$ given by Eq. (11) gives

$$(dn_1/dt)_{t=0+}=-P(n_0(0)+n_1(0)), \tag{23}$$

$$(dn_0/dt)_{t=0+}=-P(n_0(0)+n_1(0)), \tag{24}$$

where the subscript m of n corresponds to the level spacing between the $(m+1/2)$ and the $(m-1/2)$ level, and the electric field is switched on between the 3/2 and $-1/2$ level.

$n_1(0)$ in Eq. (23) and $n_0(0)$ in Eq. (24) can be estimated as 0.5 from the saturation curves with the rf field in Fig. 5. $n_0(0)$ and $n_1(0)$ in Eqs. (23) and (24) could be measured in a separate experiment or could be calculated from the Eq. (7), if all the relaxation matrix elements A_{ji} as well as $B_{ji}^{(1)}$ are known. Here it is, however, simply assumed that they are equal to unity, because the dominant relaxation mechanism in this 0.01% Cr ruby is the dipole-dipole relaxation between the Al^{27} nuclei and the Cr ions through a direct and a diffusion mechanism,[12] and therefore, the $\Delta m=\pm1$ relaxation predominates. Thus, the relation, $(dn_1/dt)_{t=0+}=(dn_0/dt)_{t=0+}$, justifies fitting the $\oplus$ and the $\triangle$ data points by a single straight line as shown in Fig. 6.

The electrically induced transition probability P was estimated from the experimental curve as

$$P=(1.0/1.5)\times10^{-6}E^2,$$

which must be equated to the square of the corresponding time-dependent off-diagonal element in Eq. (1). Since the matrix element is

$$(3/2|\mathcal{H}|-1/2)=\frac{e^2Qq}{4I(2I-1)}3\sqrt{2}\eta,$$

and the frequency difference in NMR lines between the adjacent energy spacings $\Delta\nu$, which is known to be 360 kc/sec,[10] is given by

$$\Delta\nu=\frac{e^2Qq}{I(2I-1)}\times\tfrac{3}{2};$$

η is obtained as

$$\eta=1.5\times10^{-7}\ (\mathrm{V/cm})^{-1}.$$

B. Estimation of $\partial\eta/\partial E_\perp$

The ruby lattice (α-Al_2O_r) has rhombohedral symmetry. The Al ion is located at a site whose local symmetry is C_3 and is surrounded by a distorted octahedron of oxygen ions.[14,15] Namely, the Al ion is surrounded by two O ion triangles whose planes are perpendicular to the c axis. Their centers are right above and below the Al ion, but the distances from the Al ion are not equal, their sizes are different, and their relative angles are almost but not exactly 60°. This geometry, which has no local inversion symmetry about the Al ion, provides the necessary condition for the electric field effect to be observed.[2,3]

Although a general and formal symmetry theory[3,5] gives the relations among the third-rank tensors, $\partial\varphi_{ij}/\partial E_k$, where the φ_{ij}'s are the components of the field gradient tensor with respect to the i and the j Cartesian coordinates, a specific model which will be considered here may give some physical picture of the electric field effect.

Since the local symmetry is C_3, the electric field effect can be visualized as caused by the relative polarization distortions of the oxygen triangles whose centers are on the c axis which passes through the Al ion.

If a point-charge model is assumed, a relative displacement of the surrounding ions with respect to the Al ion, $\delta\mathbf{X}$, can be expressed by

$$\delta\mathbf{X}=\mathbf{a}\cdot\mathbf{E}, \tag{25}$$

where $\mathbf{a}$ is a polarizability tensor for a particular ion at a particular site. Since the small displacement $\delta\mathbf{X}$ of the ion is equivalent to placing a dipole $e\delta\mathbf{X}$ at the position of the ion, the additional field gradient caused by the electric field at the Al ion can be calculated as the superposition of the effect of these dipoles.

If we choose a cylindrical coordinate system (r,θ,z) for the particular ion, O_1, in Fig. 7, for instance, the dis-

[14] R. W. G. Wyckoff, *Crystal Structure* (Interscience Publishers, Inc., New York, 1948), Vol. II.

[15] N. Laurance, E. C. McIrvine, and J. Lambe, J. Phys. Chem. Solids **23**, 515 (1962).

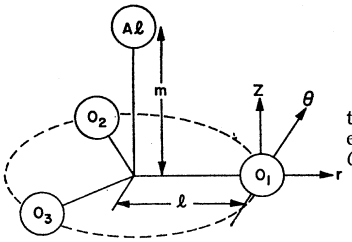

FIG. 7. The relative positions of an Al ion and three equivalent O ions about a C_3 axis.

placement of this ion is

$$\begin{bmatrix}\delta x_r\\ \delta x_\theta\\ \delta x_z\end{bmatrix}=\begin{bmatrix}a_r & a_{r\theta} & a_{rz}\\ a_{r\theta} & a_\theta & a_{\theta z}\\ a_{rz} & a_{\theta z} & a_z\end{bmatrix}\begin{bmatrix}E_r\\ E_\theta\\ E_z\end{bmatrix}. \tag{26}$$

In the present experiment E_z is equal to zero. It can be shown that (i) the net effect of the tangential displacements δx_θ of the three equivalent ions (O_1, O_2, and O_3 in Fig. 7) does not produce any first-order change in φ_{ij}; (ii) the net effect for φ_{zz}, namely, $\partial\varphi_{zz}/\partial E_\perp$ is always zero, as expected from the general symmetry argument;[2,5] and (iii) the electric field produces only an asymmetry in the initially symmetric field gradient tensor and although the directions of the principal axes of this deformed φ_{xy} depend on the direction of the applied electric field, their magnitudes are independent of the E direction.

A straightforward calculation gives

$$\delta\varphi_\pm=\pm\{[(9/4)(-3l^3+2m^2l)a_r+(45/4)l^2ma_{rz}]^2 +[(9/4)(-3l^3+2m^2l)a_{r\theta}+(45/4)l^2ma_{\theta z}]^2\}^{1/2} \times(l^2+m^2)^{-7/2}E, \tag{27}$$

where l is the distance between the center of the triangle and the ions of the triangle, and m is the distance between the Al ion and the center of the triangle as shown in Fig. 7. $\delta\varphi_+$ and $\delta\varphi_-$ are the distortions in the field gradient tensor expressed in the principal axis system in the xy plane and are related to the induced η by

$$\eta=(\delta\varphi_+-\delta\varphi_-)/\varphi_{zz}=2\delta\varphi_+/\varphi_{zz}. \tag{28}$$

The last statement (iii) implies that the magnitude of the electrically induced asymmetry parameter η does not depend on the direction of the electric field in the xy plane.

In order to estimate the $d\eta/dE_\perp$ for the ruby crystal, where E is the electric field in the xy plane, only the six neighboring oxygen ions about the Al ion are considered, a_{rz}, $a_{r\theta}$, and $a_{\theta z}$ are neglected, and a_r for the inequivalent O ions are assumed to be equal.

The asymmetry parameter thus estimated is

$$d\eta/dE_\perp=0.7a_r, \tag{29}$$

where the antishielding constant $(1-\gamma_\infty)$ is assumed to be 5 and φ_{zz} of Eq. (28) is the experimental value. The comparison with the experimental value of $d\eta/dE_\perp=1.5\times10^{-7}$ (V/cm)$^{-1}$ gives the polarizability a_r, which agrees within an order of magnitude with an estimation of a_r using dielectric constant data.[3] The crude models and the precision of the experimental data do not seem to warrant any further argument.

C. Transient Response

The transient behaviors shown in Figs. 4 and 5 could be quantitatively reproduced by the Eq. (21) if all the elements of the relaxation matrix A_{ji} were known, since the matrix for the external driving fields B_{ji} can be known from the steady-state values and the initial slope. If the A_{ji}'s were obtained, the relaxation mechanism itself could be derived from them.

One of the most convenient ways to get A_{ji} is to excite the center line $(1/2\rightleftarrows-1/2)$ with an rf field so that the center line is at least partially saturated and then observe the saturation recovery of the three lines, $(1/2\rightleftarrows-1/2)$, $(3/2\rightleftarrows1/2)$, and $(5/2\rightleftarrows3/2)$ [or the other equivalent three, $(1/2\rightleftarrows-1/2)$, $(-3/2\rightleftarrows-1/2)$, and $(-5/2\rightleftarrows-3/2)$] after the rf field is shut off. This can be done either using a spectrometer with a sufficiently weak H_1 or using a pulse method.[6] In this case, the rate equations (2) reduce to three equations,[11] because the symmetric initial conditions permit setting $n_j=n_{-j}$. The saturation recovery curves are then expressed by the linear combination of only three exponentials.

Brun *et al.*[6] observed the saturation recovery of the center line, $(1/2\rightleftarrows-1/2)$ in 0.01% ruby at 4.2°K, which corresponds to our experimental condition, after symmetric saturation. The curve (a) in Fig. (8) in their paper suggests the three exponentials. Their curve can be fitted by

$$n_0(t)=0.41e^{-0.34t}+0.51e^{-0.11t}+0.17e^{-0.018t}.$$

If the similar recovery curves for $n_1(t)$ and $n_2(t)$ or for $n_{-1}(t)$ and $n_{-2}(t)$ were observed after *the same symmetric saturation*, one could get all the necessary matrix elements A_{ji} for this sample at this temperature. Since the experimental equations give the eigenfunctions $a_j^{(k)}$ and the eigenvalues $\lambda^{(k)}$ in Eq. (19) [or in Eq. (21)], a series of equations, Eq. (20) with $B_{ji}=0$, for $k=1, 2\cdots$ with any one value of j will determine $A_{j1}, A_{j2}, \cdots$. And this would permit a comparison of A_{ji} with the theoretical matrix for spin diffusion[12] and for quadrupole relaxation.[8,11]

Since this information is not available at present, only a qualitative discussion is given for the observed transient curves.

If the electric and magnetic rf transition probabilities, P and K, respectively, have the relation,

$$P\gg K\gg A_{ji},$$

and we neglect A_{ji} in the relaxation matrix, the characteristic relaxation constants, $\lambda^{(k)}$ in Eq. (21) are easily calculated for the present case of spin 5/2 as

(i) $\lambda=0, 0, 0, 2P+\frac{1}{2}K+O(K^2/P)$, and $\frac{3}{2}K+O(K^2/P)$, or

(ii) $\lambda=0, 0, 0, 2P$, and $2K$.

The first solution (i) corresponds to the case where P and K overlap or contact, i.e., where the relation between the electric field frequency ν_E and the rf magnetic field frequency ν_M is given by

$$h\nu_E=(E_m-E_{m-2}),$$

and

$$h\nu_M=E_{m+1}-E_m,\ E_m-E_{m-1},\ E_{m-1}-E_{m-2},$$

or

$$E_{m-2}-E_{m-3};$$

solution (ii) corresponds to the other cases.

In any case, if the neglected terms A_{ji} are taken into account, it may be said that the largest of the five characteristic relaxation constants is determined predominantly by the electric field transition P, the second largest is mainly determined by K, and the remaining three represent the slow relaxations which are determined by the spin-lattice relaxation matrix elements A_{ji} and their cross terms with P and K.

In the present case since the assumption $P\gg K$ is satisfied but $K\approx A_{ji}$, the second largest relaxation constant has the same order of magnitude as the other three. Therefore when the strong rf electric field is suddenly turned on (B in Fig. 3), the signal intensity changes very rapidly first, where the initial slope is given by Eq. (22) and the subsequent time dependence is described by e^{-2Pt}. Following the initial change, the signal intensity relaxes with larger time constants of the same order of magnitude as the A_{ji}. Finally the signal approaches the steady-state values given by Eq. (14).

This may be interpreted physically as follows: the strong transition corresponding to ν_E predominates immediately after the rf electric field is turned on, and then the redistribution of population among all the levels follows with time constants of the order of the A_{ji}'s.

It is noted that since the amplitude and the sign of each normal mode of relaxation are dependent on the initial conditions, the transient curves are not necessarily monotonic with respect to time and some of the normal modes do not show up for particular initial conditions. There is no sharp initial change, for instance, in the noncrossing cases, $[\nu_E=(5/2\rightleftarrows 1/2);\ \nu_M=(-1/2\rightleftarrows -3/2)$, or $\nu_M=(-3/2\rightleftarrows -5/2)]$ and $[\nu_E=(3/2\rightleftarrows -1/2);\ \nu_M=(-3/2\rightleftarrows -5/2)]$ in Figs. 4 and 5, because of the vanishing $B_{ji}^{(2)}$ in Eq. (22), which indicates that the fastest relaxation mode is very small. Only the slow redistribution processes are observed in these cases. Another example of the preferential excitation is the case of the symmetric saturation shown previously, where only three modes out of five, the fastest, the third fastest, and the slowest mode, are observed.[6,11,12]

The direction of the initial sharp change for each case in Figs. 4 and 5 agrees with what is expected from Eq. (22).

D. Line Shape of Nuclear Electric Resonance

The nuclear electric resonance line observed by means of the double resonance technique is considerably larger in width than the straight NMR line and is asymmetric in shape as shown in Fig. 2. The half-width of the former is about 25 kc/sec, whereas the width of the NMR lines is only about 8 kc/sec.[10]

Each NMR line has a fine structure, which, except for the center line, is not symmetric. These structures have been interpreted in terms of the dipole-dipole interaction between the nearest neighbor Al nuclei.[10]

The calculation similar to that in reference 10 was carried out for the $(5/2\rightarrow 1/2)$ nuclear electric resonance line. The result derived from the dipole-dipole interaction between the nearest neighbor Al^{27} pair is shown in Fig. 8.

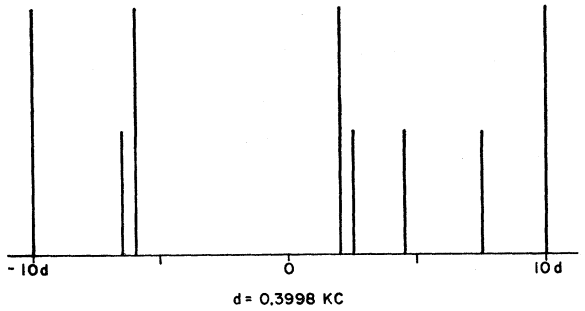

FIG. 8. The dipolar fine structure of $(5/2\rightleftarrows 1/2)$ line calculated in terms of the nearest neighbor dipole interaction.

It is noted that the dipole linewidth is about twice as big as that of the NMR lines shown in Fig. 2 of reference 10. This is understood physically as follows: The energy levels of the Al^{27} nucleus, which are specified by m_z, are split into five fine structure components by the local dipole magnetic field of the nearest neighbor Al nucleus. The splitting is proportional to m_z. Therefore, the linewidth of the $\Delta m=2$ line is twice as big as that for the $\Delta m=1$ line. This pictorial model merely illustrates the linewidths and does not consider in detail the dipole-dipole Hamiltonian.

The calculated dipole structure is asymmetric as is the case for the $\Delta m=\pm 1$ lines. The observed linewidth is, however, about three times as much as the observed NMR lines. One of the reasons for this extra broadening is that the linewidth of each component line in Fig. 8 is larger than that for the $\Delta m=1$ line for the same reason as stated above. The other reason is the fact that since the rf electric field is so strong as to reverse the intensity of the monitor signal near the center of the line, the response of the monitor signal is not linear with respect to the line shape of the $\Delta m=\pm 2$ transition. The peak of the observed line shape in Fig. 2 may be squashed appreciably, and the apparent half-width may be wider than the real width.

The direction of asymmetry of the line shape is determined by the relative signs of the g value and the

quadrupole coupling constant for the Al^{27} nucleus. Since the former sign is known, the sign of the quadrupole coupling constant can be derived as positive in agreement with the conclusion in reference 10.

SUMMARY

The electrically induced nuclear resonance was observed for Al^{27} in a ruby single crystal using nuclear double resonance technique. The line shape is asymmetric, and its width is more than twice as much as the straight NMR lines. The shape and the width are interpreted in terms of the nearest neighbor dipole interaction. The direction of the asymmetry agrees with the previously determined sign of the quadrupole coupling constant. The transient response of the monitor NMR signal was observed. The initial rise (or fall) time gives the transition probability of the electrically induced nuclear quadrupole transition. The transition probability thus obtained gives the magnitude of an electrically induced asymmetry parameter η in the field gradient tensor. The induced η is tentatively interpreted in terms of the polarization displacements of the surrounding ions accompanied by the external electric field.

The entire transient curves can be divided into two parts: the initial rapid change which is predominantly determined by the electric excitation and the following slow change which takes place in a time comparable with the spin-lattice relaxation time. The qualitative behavior of the transient curves is interpreted using the normal relaxation modes. The normal mode formalism is extended so as to include the external driving field.

ACKNOWLEDGMENTS

The authors would like to acknowledge the valuable discussions with Dr. J. J. Lambe. B. Poindexter assisted with the experimental setup and in taking the data.

APPENDIX

When the spin diffusion is the relaxation mechanism, Simmons *et al.*[12] have shown that the spin-lattice relaxation matrix A_{ji} in Eq. (2) contains the operator ∇^2 as is shown in Eq. (34) in their article. It is shown that this operator can be approximately replaced by c numbers as follows.

The rate equation which must be considered is

$$\partial n_j/\partial t=\sum_i A_{ji}^{(0)}n_i, \tag{A1}$$

where $n_j=n_j(\mathbf{r}t)$ is a local population difference at the position $\mathbf{r}$. Further

$$A_{ji}^{(0)}=A_{ji}+A_{ji}'\nabla^2, \tag{A2}$$

where A_{ji} and A_{ji}' are c-number matrix elements whose values are given in Eq. (34) in reference 12.

The solution of (Al) has the form[12]

$$n_j=\sum_k \alpha_j^{(k)}\Phi^{(k)}(\mathbf{r})\exp(-\lambda^{(k)}t). \tag{A3}$$

Inserting Eq. (A3) into Eq. (A1) and integrating them with respect to $\mathbf{r}$, one obtains

$$\sum_i(\lambda^{(k)}\alpha_j^{(k)}\delta_{ji}+A_{ji}\alpha_i^{(k)}+A_{ji}'\alpha_i^{(k)}d^{(k)})=0, \tag{A4}$$

where

$$d^{(k)}\equiv\int\nabla^2\Phi^{(k)}(\mathbf{r})d\mathbf{r}\Big/\int\Phi^{(k)}d\mathbf{r}. \tag{A5}$$

Equation (A4) is approximately satisfied by $\Phi^{(k)}(\mathbf{r})$ and $\lambda^{(k)}$ in Eq. (37) of reference 12 as shown by Simmons. From the $\lambda^{(k)}$ one can determine the eigenfunctions of $\alpha_j^{(k)}$.

If we assume that $\det|\alpha_j^{(k)}|$ is not zero, then we can obtain a matrix β_{ij} which satisfies the relation

$$\alpha_i^{(k)}d^{(k)}=\sum_j\beta_{ij}\alpha_j^{(k)}. \tag{A6}$$

For any one value of i we can write the k equations represented in (A6) from which the β_{i1}, β_{i2}, $\cdots$ can be deduced; hence, all β_{ij} can be evaluated. By further defining $A_{ji}''=\sum_l A_{jl}\beta_{li}$, Eq. (A4) can be reduced to

$$\sum_i(\lambda^{(k)}\delta_{ji}+A_{ji}+A_{ji}'')\alpha_i^{(k)}=0. \tag{A7}$$

The matrix elements $(A_{ji}+A_{ji}'')$ are, therefore, the required c numbers.